Ultrasmall Water-Soluble and Biocompatible Magnetic Iron Oxide Nanoparticles as Positive and Negative Dual Contrast Agents

Zhen Li, Pei Wei Yi, Qiao Sun, Hao Lei, Hong Li Zhao, Zhong Hua Zhu, Sean C. Smith, Min Bo Lan, and Gao Qing (Max) Lu**

Monodispersed water-soluble and biocompatible ultrasmall magnetic iron oxide nanoparticles (UMIONs, D = 3.3 ± 0.5 nm) generated from a high-temperature coprecipitation route are successfully used as efficient positive and negative dual contrast agents of magnetic resonance imaging (MRI). Their longitudinal relaxivity at 4.7 T (r_1 = 8.3 mM^{-1} s^{-1}) is larger than that of clinically used T_1-positive agent Gd-DTPA (r_1 = 4.8 mM^{-1} s^{-1}), and three times that of commercial contrast agent SHU-555C (r_1 = 2.9 mM^{-1} s^{-1}). The transversal relaxivity (r_2 = 35.1 mM^{-1} s^{-1}) is six times that of Gd-DTPA (r_2 = 5.3 mM^{-1} s^{-1}), half of SHU-555C (r_2 = 69 mM^{-1} s^{-1}). The in vivo results show that the liver signal from T_1-weighted MRI is positively enhanced 26%, and then negatively decreased 20% after injection of the iron oxide nanoparticles, which is stronger than those obtained from Gd-DTPA (<10%) using the same dosage. The kidney signal is positively enhanced up to 35%, similar to that obtained from Gd-DTPA. Under T_2-weighted conditions, the liver signal is negatively enhanced ≅70%, which is significantly higher than that from Gd-DTPA (≅6%). These results demonstrate the great potential of the UMIONs in dual contrast agents, especially as an alternative to Gd-based positive contrast agents, which have risks of inducing side effects in patients.

1. Introduction

In the past decades, magnetic resonance imaging (MRI) has been used as a powerful and indispensable tool in medical research, clinical diagnosis, and patient care due to its high spatial resolution and non-limited penetration depth.[1] The performance of MRI not only depends on the instrument and different imaging methodology but is also strongly determined by contrast agents, which can significantly improve the image contrast of biological targets from surrounding tissues. Contrast agents can shorten longitudinal (or spin-lattice) and transverse (or spin-spin) relaxations of protons, which respectively lead to positive enhancement (i.e., brighter image) in T_1-weighted MRI and negative enhancement (i.e., darker image) in T_2-weighted MRI in comparison with pre-contrast images.[2,3] The spin-lattice relaxation represents an energy loss of protons from the excited states to the initial states, and the spin-spin relaxation is due to the loss of phase coherence in the processing protons. Their corresponding relaxation times and relaxivities are defined as T_1, T_2 and r_1, r_2, respectively. According to these parameters, contrast agents are conventionally classified into T_1-positive agents which have similar r_1 and r_2 values, and a small r_2/r_1 ratio, and T_2-negative agents, which have an r_1 that is much smaller than r_2 (i.e., $r_1 << r_2$).

Both T_1-positive and T_2-negative contrast agents have their own advantages and disadvantages. For example, the conventional gadolinium (Gd)-based positive agents (e.g., gadolinium diethylenetriaminopentaacetic acid (Gd-DTPA)) have been extensively used because of strong paramagnetism of Gd^{3+}, leading to excellent enhancement.[4,5] But they have risks of inducing nephrogenic systemic fibrosis (NSF) in patients with

Dr. Z. Li, Prof. G. Q. (M.) Lu
ARC Centre of Excellence for Functional Nanomaterials
Australian Institute for Bioengineering and Nanotechnology
The University of Queensland
QLD 4072, Australia
E-mail: z.li3@uq.edu.au; m.lu@uq.edu.au
P. W. Yi, Prof. H. Lei
State Key Laboratory of Magnetic Resonance and Atomic and Molecular Physics
WuHan Institute of Physics & Mathematics
Chinese Academy of Sciences
WuHan 430071, P. R. China
Dr. Q. Sun, Prof. S. C. Smith
Centre for Computational Molecular Science
Australian Institute for Bioengineering and Nanotechnology
The University of Queensland
QLD 4072, Australia
Dr. H. L. Zhao, Prof. M. B. Lan
Shanghai Key Laboratory of Functional Materials Chemistry
East China University of Science and Technology
Shanghai 200237, P. R. China
Prof. Z. H. Zhu
School of Chemical Engineering
The University of Queensland
QLD 4072, Australia

DOI: 10.1002/adfm.201103123

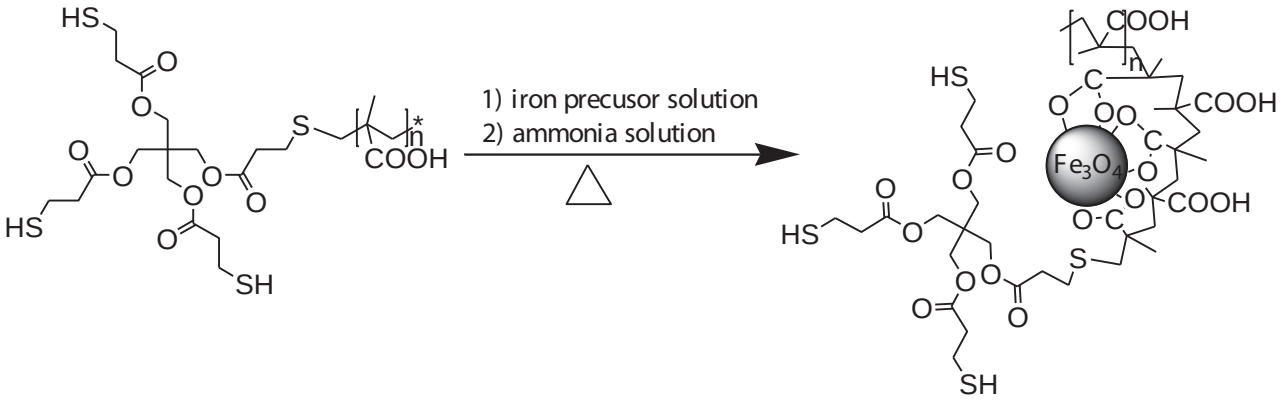

Scheme 1. Preparation of ultrasmall magnetic iron oxide nanoparticles.

impaired kidney function, especially for older patients.[6] Therefore, development of alternative T_1-positive contrast agents has been a subject of intensive research. Manganese (Mn) complexes, MnO, and FeCo nanoparticles have shown their potential in this aspect.[7–9] However, the accumulative toxicity arising from Mn and Co might limit their clinical applications.

In terms of low toxicity, magnetic iron oxide nanoparticles have been proven to be one of the most promising contrast agents for clinical use because they are naturally found in human body.[3,10–12] However, most iron oxide nanoparticles have a large r_2/r_1 ratio and are used as negative contrast agents. They can be detected in a smaller concentration and a submillimeter area with T_2* or susceptibility weighted imaging in comparison with T_1-positive contrast agents. But the lack of specificity in heterogeneous anatomy and potential confusion with signals from bleeding, calcification, metal deposits (such as endogenous iron), and other susceptibility artifacts limit their applications.[10]

Therefore, it is highly desirable and a great challenge to prepare robust dual contrast agents for overcoming the disadvantages of single modality contrast agents. The simultaneous use of positive and negative MRI imaging that employs the same contrast agents will significantly improve the detection accuracy. In this article, we prepare monodsipersed water-soluble and biocompatible ultrasmall magnetic iron oxide nanoparticles (UMIONs, D = 3.3 nm) through a high-temperature coprecipitation method and exploit their applications in positive and negative dual contrast agents of MRI. Both in vitro and in vivo results show their excellence in T_1 and T_2-weighted MRI imaging.

2. Results and Discussion

Magnetic iron oxide based negative contrast agents are conventionally prepared by aqueous or non-aqueous routes.[13–19] The aqueous routes such as coprecipitation usually generate nanoparticles with a broad size distribution and low crystallinity. The non-aqueous routes, such as the thermal decomposition approach, can produce monodispersed nanoparticles with high crystallinity. However, most magnetic iron oxide nanoparticles obtained from these methods have a large particle size (D > 5.0 nm) and a large r_2/r_1 ratio, not suitable for T_1-weighted positive imaging. Very recently, there are a few reports on preparation of ultrasmall magnetic iron oxide nanoparticles (UMIONs, D < 5.0 nm) which show potential in positive MRI imaging.[20–23] For example, the Hyeon group prepared organic-soluble UMIONs in a range of ≈1.5–3 nm using a high-temperature thermal decomposition method and then modified them with functional poly(ethylene glycol) (PEG) to result in contrast agents for T_1-weighted positive imaging.[22]

In contrast to the thermal decomposition of organometallic precursors in organic solvents, we developed a high-temperature coprecipitation method for synthesis of monodsipersed water-soluble UMIONs without post surface modification, in which poly(acrylic acid), poly(methacrylic acid) and their derives were used as versatile stabilizers.[23] These polymer ligands can effectively prevent the aggregation of nanoparticles to ensure a small particle size, and provide reactive groups for introducing other functions. Here we use thiol functionalized poly(methacrylic acid) (PMAA-PTTM, M_n = 6359 g mol^{-1}, M_w = 7524 g mol^{-1}) as a stabilizer, which shows better control of particle size and size distribution compared with other polymers (**Scheme 1**). In addition, we use concentrated HCl to dissolve iron precursors in order to prevent their hydrolysis and condensation before the addition of precipitating agents. **Figure 1**a and Figure S1 (Supporting Information) show transmission electron microscopy (TEM) images of obtained nanoparticles. These nanoparticles show a size of 3.3 ± 0.5 nm, which is smaller than our previous report (D = 4.5 ± 0.5 nm).[23] The narrow size distribution is attributed to a burst of nucleation and strong coordination ability of polymer ligands, which leads to the separation of nucleation and growth processes and results in monodispersed nanoparticles.[23]

High-resolution TEM (HRTEM) image in Figure 1b clearly shows the lattice of nanoparticles, indicating them as being well crystallized despite of the small size. This is attributed to the higher reaction temperature (100 °C) in comparison with conventional coprecipitation, which is usually performed at room temperature.[16] The inset in Figure 1b exhibits lattice fringes with characteristic interplanar spacings of 0.21 nm and 0.17 nm, corresponding to (400) and (422) planes of Fe_3O_4, respectively. The high crystallinity of nanoparticles is also proved by their well-resolved X-ray diffraction peaks (Figure S2, Supporting

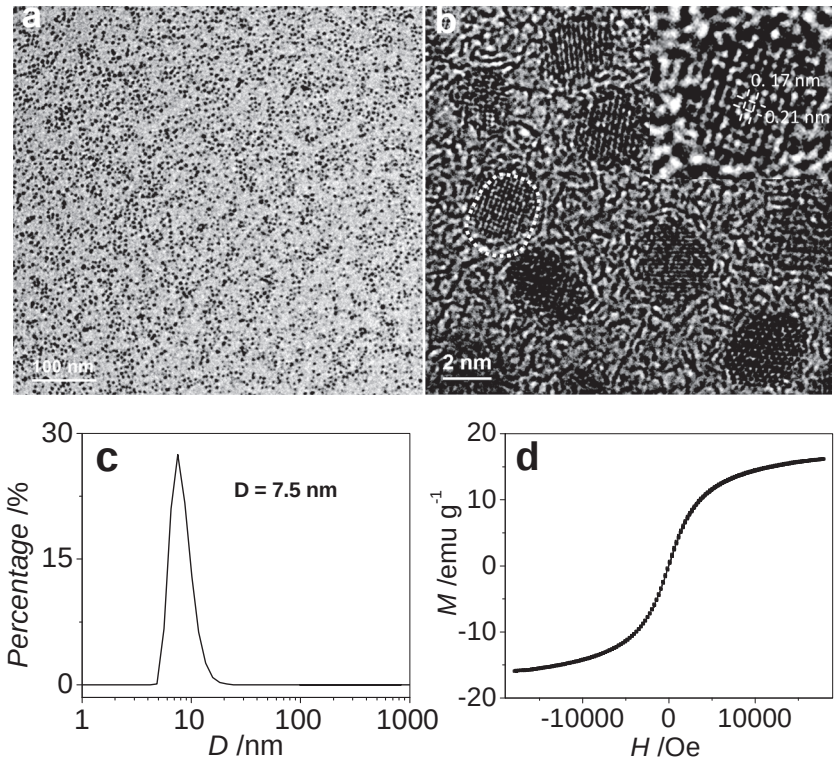

Figure 1. a,b) TEM and HRTEM images of ultrasmall iron oxide nanoparticles. The insert is a magnified particle labeled with white cycle. c,d) Hydrodynamic size and magnetization curve of these nanoparticles measured at room temperature.

Information), which match well with those of Fe_3O_4 (JCPDS: 01-071-6336). The Fe^{3+}/Fe^{2+} ratio in nanoparticles is determined to be 2.39 by titration, which slightly deviates from stoichiometric ratio. This might be attributed to the oxidation of nanoparticles during long-term dialysis (72 h). These nanoparticles show excellent water-solubility and their hydrodynamic size is 7.5 nm (Figure 1c), as determined by dynamic light scattering (DLS). They also display superparamagnetism with a magnetization of 16 emu g^{-1} sample at room temperature (Figure 1d).

The small hydrodynamic size indicates that they belong to very small superparamagnetic iron oxide particles (VSOP, D_{hydro} < 20 nm) and show great potential in MRI contrast agents.[11] We thereby measured their relaxivity and **Figure 2** shows T_1-, T_2-weighted MRI images and relaxivity of their saline solutions recorded on a 4.7 T MRI scanner at room temperature. Both T_1- and T_2-weighted images demonstrate the strong dependence of signal intensity on iron concentration. The longitudinal relaxivity (r_1) is 8.3 mM^{-1} s^{-1}, which is about three times of that from commercial contrast agent SHU-555C (r_1 = 2.9 mM^{-1} s^{-1}).[24] The transversal (r_2) relaxivity is 35.1 mM^{-1} s^{-1}, which is only

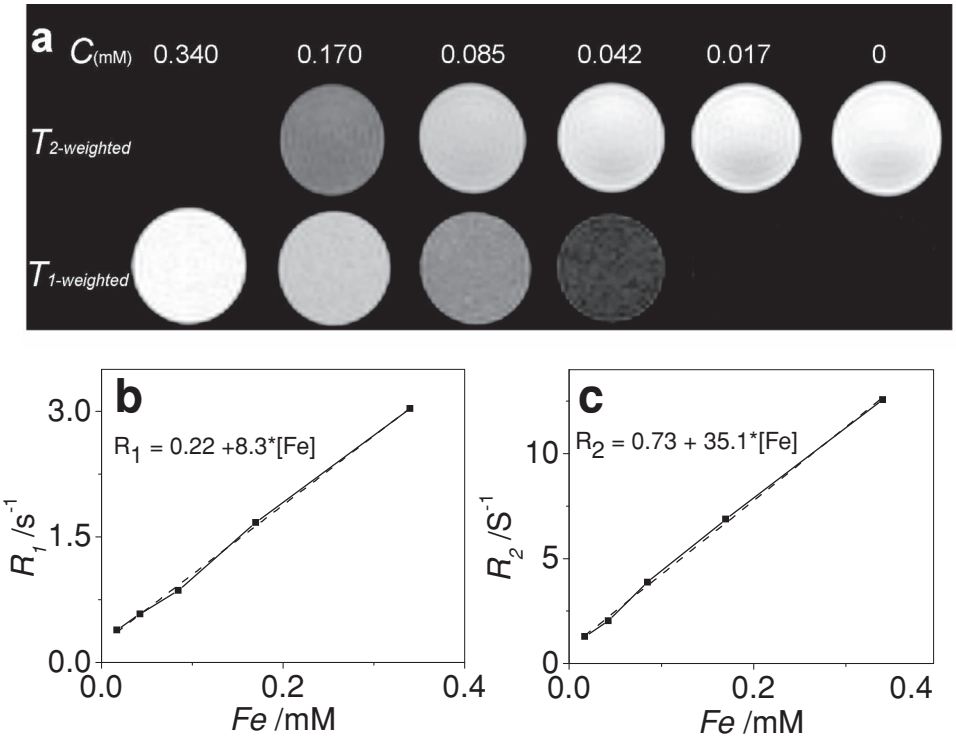

Figure 2. In vitro T_1- and T_2-weighted images and relaxivity of 3.3 nm UMIONs recorded on a 4.7 T scanner.

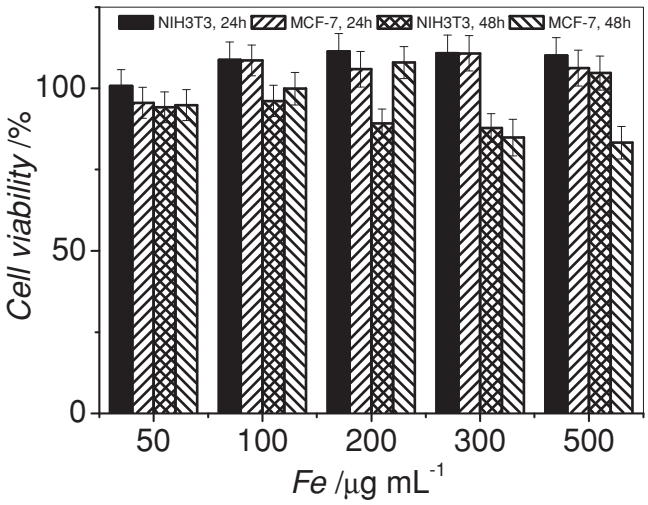

Figure 3. Viability of NIH3T3 and MCF-7 cells after incubated with 3.3 nm UMIONs with different Fe concentrations for 24 h and 48 h.

half of SHU-555C (r_2 = 69 mM^{-1} s^{-1}).[24] The pronounced longitudinal relaxivity and small r_2/r_1 ratio (r_2/r_1 = 4.2) of our UMIONs suggest their potential as dual contrast agents, especially as T_1-positive contrast agents. Therefore, we compare their relaxivities with the commercial T_1-positive agent Gd-DTPA. Figure S3 (Supporting Information) shows T_1-, T_2-weighted MRI images and relaxivities of Gd-DTPA measured at 4.7 T using the same parameters. The resultant r_1 and r_2 relaxivities of Gd-DTPA are, respectively, 4.8 and 5.3 mM^{-1} s^{-1}, which are much smaller than our UMIONs (r_1 = 8.3 mM^{-1} s^{-1}; r_2 = 35.1 mM^{-1} s^{-1}). The relaxivities of these agents were also measured at 1.5 T clinically used magnetic field. The r_1 and r_2 of our UMIONs are 11.7 mM^{-1} s^{-1} and 28.5 mM^{-1} s^{-1}, respectively, which are respectively three times and seven times of Gd-DTPA agent (r_1 = 3.3 mM^{-1} s^{-1}; r_2 = 3.9 mM^{-1} s^{-1}) measured under the same conditions. These values are also comparable with previous reports from other groups.[20–22] The large longitudinal relaxivity of our nanoparticles is attributed to their relatively small size (D = 3.3 nm) which leads to weak magnetism[22] due to the increasing surface disorder caused by surface spin canting effects.[25]

In order to assess the toxicity of our UMIONs for in vivo MRI imaging, we did an MTT (3-(4, 5-dimethylthiazol2-yl)-2, 5-diphenyltetrazolium bromide)assay using the mouse fibroblast cell line NIH3T3 and human breast adenocarcinoma cell line MCF-7 as models. **Figure 3** shows cell viability after incubated with UMIONs at different concentrations (0–500 μg[Fe] mL^{-1}) for 24 h and 48 h. The viability of both cells exceeded 95% in all investigated concentrations after 24 h incubation. Prolonging incubation to 48 h led to a slight decrease in cell viability at high concentration, which is still more than 83%. These results demonstrate little toxicity of our nanoparticles as dual contrast agents.

On the basis of above in vitro results, we performed in vivo MRI experiments on live mouse using UMIONs as contrast agents. We first conducted conventional negative MRI imaging and Figure S4 (Supporting Information) shows the typical T_2-weighted images of mouse liver and kidney collected at different intervals after injection of UMIONs with a dosage of 0.041 mmol[Fe] kg^{-1} (200 μL, 5.44 mM [Fe]). In comparison with pre-contrast images, the liver signal intensity decreased by 78% after 155 min injection, and then remained almost unchanged till the end of experiment (605 min). The kidney signal intensity dropped by 15% in the first 15 min, then partially recovered and finally slightly increased with 11%. These results suggest the T_1-effects of our nanoparticles, even performed with T_2-weighted MRI parameters.

In order to further demonstrate their T_1-effect, we repeated the experiment and recorded the T_1- and T_2-weighted images by an alternate scanning manner. Different to previous case, the dosage was decreased to 0.019 mmol[Fe] kg^{-1} and was injected in four shots with 2 h intervals between two successive injections (4 × 100 μL, 1.36 mM [Fe]). **Figure 4** shows T_1- and T_2-weighted MRI images of liver and kidney. The signal intensity

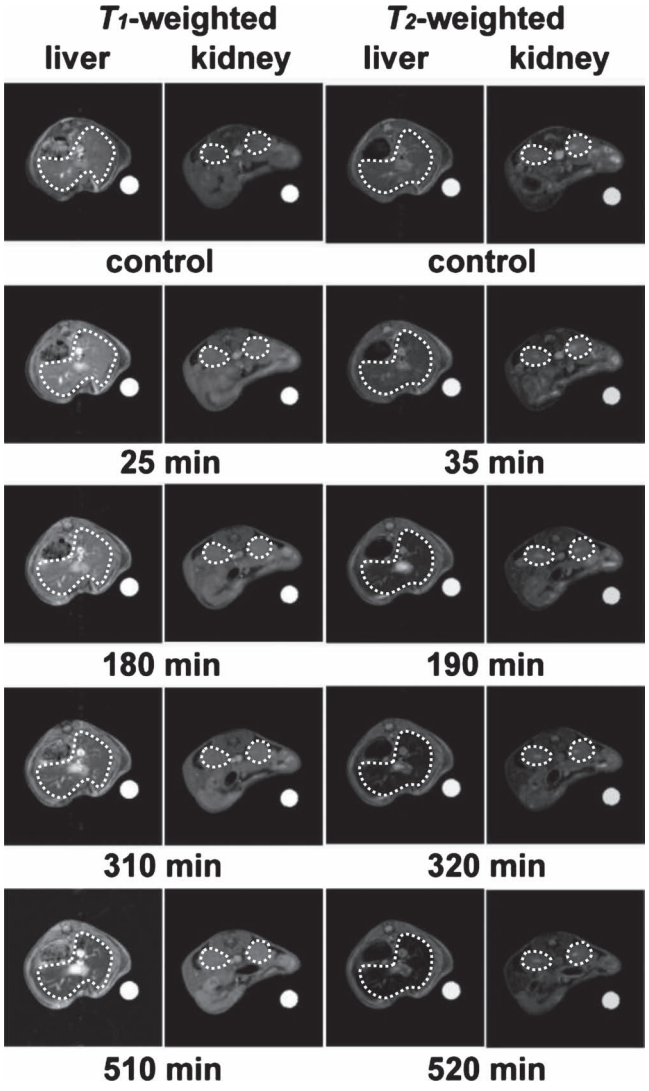

Figure 4. In vivo T_1- and T_2-weighted images of mouse liver and kidney (selected area) collected from different time by alternate scanning.

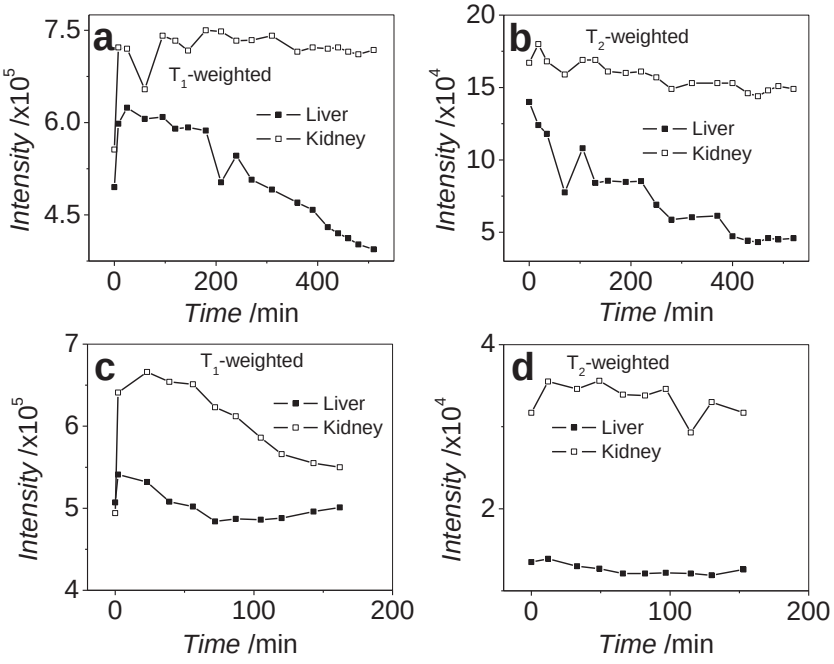

Figure 5. Signal intensity of T_1- and T_2-weighted images (Figure 4 and Figure S5 (Supporting Information)) of liver and kidney obtained from same dosage of a,b) 3.3 nm UMIONs and c,d) Gd-DTPA agents using the same scanning parameters.

of labeled areas was plotted in **Figure 5**. For T_1-weighted images, the liver become brighter as compared with precontrast image after the first shot of UMIONs, and the signal increased by 26% after 25 min injection (Figure 5). Then the images gradually changed from bright into dark with the decrease of signal intensity due to the particle accumulation. The liver remained bright for 300 min until the third shot of nanoparticles, and the final signal intensity decreased by 20% after the fourth shot. In contrast, the kidney images always kept bright and the signal was enhanced more than 17% and the maximum enhancement was up to 35% (Figure 5). Similar to the case of high dosage (0.041 mmol [Fe] kg^{-1}), the T_2-weighted liver images became darker and darker with the decrease of signal intensity. The signal decreased by 69% after four shots of UMIONs. For T_2-weighted kidney images, the signal slightly increased first (≈7%) and then decreased (≈14%).

The above in vivo results demonstrate that positive and negative enhancement of MRI can be achieved using our nanoparticles as dual contrast agents. Particular attention should be paid to positive enhancement because it was immediately observed after injection of these UMIONs using a conventional spin echo sequence, i.e., multi-slice multi-echo (MSME). This is a huge improvement to the work reported earlier in which positive enhancement of iron oxide nanoparticles was observed with new MRI imaging techniques[26,27] and it is typically required to wait for ≈24 to 72 h to do positive enhanced imaging after injection.[28]

In order to demonstrate the potential of our nanoparticles as an alternative to Gd-based T_1-positive agents, we compare the in vivo enhancement efficiency of our UMIONs with clinically used Gd-DTPA. It should be noted that the signal enhancement was negligible if the Gd-DTPA was divided into four shots. Therefore we injected the same dosage of Gd-DTPA via a single shot (400 µL, 1.0 mM [Gd]) and Figure S5 (Supporting Information) presents the T_1- and T_2-weighted MRI images of liver and kidney obtained under the same scanning parameters. The variation of signal intensity was plotted in Figure 5c,d. It can be seen that the T_1-weighted MRI images of both liver and kidney become bright in a time shorter than our magnetic nanoparticles, i.e., 2 min versus 25 min for liver and 23 min versus 95 min for kidney. The shorter enhancement time of Gd-DTPA is attributed to their fast pharmacokinetics due to the small size and low molecular weight.[4,5] In addition, the liver signal only increased by 6.7% with Gd-DTPA, which is lower than our magnetic nanoparticles (26%). Meanwhile, the maximal kidney signal increased by 35%, which is the same to our nanoparticles. For the T_2-weighted MRI images, there is no significant difference among the liver images before and after injection of Gd-DTPA. However, the kidney signal was improved by 10% under T_2-weighted conditions, indicating that Gd-DTPA is only suitable as T_1-positive contrast agents. It should be noted that all the mice used recovered from anesthesia spontaneously after the experiment and lived normally, which supports the biocompatibility and little toxicity of our UMIONs.

3. Conclusions

In summary, water-soluble and biocompatible monodispersed UMIONs have been synthesized via a high-temperature co-precipitation method using thiol-functionalized poly(methacrylic acid) as stabilizer. These magnetic nanoparticles have been used as efficient T_1- and T_2-contrast agents, by in vitro and in vivo comparing with clinically used Gd-DTPA agents. The in

vitro results show that their longitudinal (r_1) and transversal (r_2) relaxivities are larger than those of Gd-DTPA agent, respectively. The in vivo results demonstrate the better performance of our nanoparticles in T_1- and T_2-weighted MRI imaging than Gd-DTPA. This investigation shows the great potential of UMIONs in dual contrast agents of MRI, especially as an alternative to Gd-based T_1-contrast agents with known clinical risks.

4. Experimental Section

Materials: $FeCl_3{\cdot}6H_2O$, $FeSO_4{\cdot}7H_2O$, $NH_3{\cdot}H_2O$ (28%) and concentrated HCl (37%) were purchased from Aldrich and used as received. Thiol-functionalized poly(methacrylic acid) (PMAA-PTMP) was prepared as described elsewhere.[23,29–31] NaCl (0.9%) and Gd-DTPA (0.5 M) were ordered from Beijing BeiLu Pharmaceutical Co. Ltd. Mouse fibroblast cell line NIH3T3 and human breast adenocarcinoma cell line MCF-7 were obtained from Institute of Biochemistry and Cell Biology (Shanghai, China). White Kunming mice with weight between 22 and 30 g were purchased from Wuhan Institute of Biological Products (China).

Synthesis of Ultrasmall Magnetic Iron Oxide Nanoparticles (UMIONs): PMAA-PTMP (0.1747 g, number-molecular-weight (M_n) is 6359 g mol^{-1} and weight-molecular-weight (M_w) is 7524 g mol^{-1}) was dissolved in Milli-Q water (50 mL) and purged with nitrogen to remove oxygen. The polymer solution was then heated to reflux. Meanwhile, $FeCl_3{\cdot}6H_2O$ (0.1378 g, 0.51 mmol) and $FeSO_4{\cdot}7H_2O$ (0.0701 g, 0.252 mmol) were dissolved in concentrated HCl (1 mL). Then the mixture of iron precursors was quickly injected into the hot polymer solution, followed by the addition of concentrated ammonia solution (15 mL, 28%). The solution became black immediately and the resultant black solution was refluxed for 2 h before cooled down. The solution was concentrated and then dialyzed against Mili-Q water (the molecular weight cut-off was 10 000 g mol^{-1}) for 72 h to remove impurities. The dialyzed solution was then evaporated under reduced pressure and the dried UMIONs were collected with a permanent magnet.

Characterizations: Low-resolution TEM images were collected on a JEOL-1010 electron microscope operating at an accelerating voltage of 100 kV. HRTEM images were recorded on a JEOL-2100 electron microscope operating at an accelerating voltage of 200 kV. X-ray diffraction (XRD) patterns were measured using a Bruker D8 Advanced Diffractometer at 40 kV and 30 mA using Cu Kα1 radiation (λ = 1.54056 Å). Hydrodynamic size of magnetic nanoparticles was determined with a ZETASIZER. Magnetic properties were recorded on a Quantum Design MPMS SQUID magnetometer.

MTT Assay: Both NIH3T3 and MCF-7 cell lines were seeded into a 96-well plate in culture medium (100 µL). After 24 h, various concentrations of UMIONs (200 µL, 0–500 µg mL^{-1}) was added into each well. Each concentration was set in six wells to provide statistically reliable results. The cells were cultured at 37 °C in a 5% CO_2 incubator. After 24 h (48 h) incubation with UMIONs, the medium was removed and 3-(4, 5-dimethylthiazol2-yl)-2, 5-diphenyltetrazolium bromide (MTT) (100 µL, 0.5 mg mL^{-1}) was added into each well. Following incubation for another 4 h, the medium was removed and dimethyl sulfoxide (DMSO, 100 µL) was added into each well. The optical density (OD) value was determined using an enzyme-linked immunosorbent assay plate reader at wavelengths of 492 and 630 nm. The cell viability was assessed by the ratio of OD values from each group and control group.

In Vitro MRI Measurements: Magnetic nanoparticles were dissolved in 0.9% NaCl to form stock solution (43.2 mM [Fe]) and then diluted into different concentrations for measuring the T_1 and T_2 relaxation. The measurements were respectively carried out on a 4.7 T Bruker Biospec Avance spectrometer and a 1.5 T Bruker mq60 NMR Analyzer. The MSME method was used for 4.7 T MRI scanner, and the parameters used for T_1-weighted imaging were: echo time (TE) = 11 ms; repetition time (TR) = 300 ms; matrix size = 128 × 128; field of view (FOV) = 4.0 × 4.0 cm^2; and slice thickness is 1 mm. The T_2-weighted measurements were performed under the same conditions except of longer TE (30 ms) and TR (3000 ms). For mq60 Analyzer, Carr-Purcell-Meiboom-Gill (CPMG) pulse sequence (T_{cp} = 0.5 ms) and inversion recovery pulse sequence (T_{cp} = 5 ms) were respectively applied for T_2 and T_1 measurements. In order to demonstrate the efficiency of magnetic iron oxide nanoparticles in MRI imaging, clinically used Gd-TDPA agents were diluted into different concentrations and then their T_1- and T_2-relaxation were measured on the 4.7 T scanner and the 1.5 T Analyzer using the same parameters.

In Vivo MRI Measurements: The in vivo T_1- and T_2-weighted MRI images were recorded on the 4.7 T Bruker Biospec Avance spectrometer. The dosage was calculated on the basis of metal concentration. The mouse was anesthetized with isoflurane and fixed inside magnet bore. Then contrast agents were administered by tail vein injection after the mouse became stabilized. The alternating T_1- and T_2-weighted MRI were carried out using MSME method. The scanning parameters used were similar to the in vitro MRI imaging except of different TE and TR. The TE and TR of T_1-weighted images were respectively 9 ms and 150 ms, while for T_2-weighted images TE and TR were 30 ms and 2000 ms.

Supporting Information

Supporting Information is available from the Wiley Online Library or from the author.

Acknowledgements

Z.L. gratefully acknowledges the scientific visit to China sponsored by Australia Academy of Science, and the award of a Queensland Smart Future Fellowship, a University of Queensland (UQ) early-career-research (ECR) grant and a UQ new staff research startup grant. Support from the Australian Research Council (through its centres program) to the ARC Centre of Excellence for Functional Nanomaterials is also gratefully acknowledged. H.L. acknowledges the support from Natural Science Foundation of China grant (20921004).

Received: December 23, 2011
Published online: March 15, 2012

[1] R. Weissleder, M. J. Pittet, *Nature* **2008**, *452*, 580.
[2] H. B. Na, I. C. Song, T. Hyeon, *Adv. Mater.* **2009**, *21*, 2133.
[3] Y. W. Jun, J. H. Lee, J. Cheon, *Angew. Chem. Int. Ed.* **2008**, *47*, 5122.
[4] H. J. Weinmann, R. C. Brasch, W. R. Press, G. E. Wesbey, *Am. J. Roentgenol.* **1984**, *142*, 619.
[5] S. Aime, M. Botta, E. Terreno, *Adv. Inorg. Chem.* **2005**, *57*, 173.
[6] P. H. Kuo, E. Kanal, A. K. Abu-Alfa, S. E. Cowper, *Radiology* **2007**, *242*, 647.
[7] H. B. Na, T. Hyeon, *J. Mater. Chem.* **2009**, *19*, 6267.
[8] H. B. Na, J. H. Lee, K. J. An, Y. I. Park, M. Park, I. S. Lee, D. H. Nam, S. T. Kim, S. H. Kim, S. W. Kim, K. H. Lim, K. S. Kim, S. O. Kim, T. Hyeon, *Angew. Chem. Int. Ed.* **2007**, *46*, 5397.
[9] W. S. Seo, J. H. Lee, X. Sun, Y. Suzuki, D. Mann, Z. Liu, M. Terashima, P. C. Yang, M. V. Mcconnell, D. G. Nishimura, H. Dai, *Nat. Mater.* **2006**, *5*, 971.
[10] J. W. M. Bulte, D. L. Kraitchman, *NMR Biomed.* **2004**, *17*, 484.
[11] C. Corot, P. Robert, J. M. Idee, M. Port, *Adv. Drug Delivery Rev.* **2006**, *58*, 1471.
[12] M. Mahmoudi, H. Hosseinkhani, M. Hosseinkhani, S. Boutry, A. Simchi, W. S. Journeay, K. Subramani, S. Laurent, *Chem. Rev.* **2010**, *111*, 253.
[13] S. H. Sun, H. Zeng, *J. Am. Chem. Soc.* **2002**, *124*, 8204.
[14] T. Hyeon, *Chem. Commun.* **2003**, 927.

[15] A.-H. Lu, E. L. Salabas, F. Schth, *Angew. Chem. Int. Ed.* **2007**, *46*, 1222.
[16] S. Laurent, D. Forge, M. Port, A. Roch, C. Robic, L. V. Elst, R. N. Muller, *Chem. Rev.* **2008**, *108*, 2064.
[17] Z. Li, H. Chen, H. B. Bao, M. Y. Gao, *Chem. Mater.* **2004**, *16*, 1391.
[18] Z. Li, Q. Sun, M. Y. Gao, *Angew. Chem. Int. Ed.* **2005**, *44*, 123.
[19] Z. Li, L. Wei, M. Y. Gao, H. Lei, *Adv. Mater.* **2005**, *17*, 1001.
[20] U. I. Tromsdorf, O. T. Bruns, S. C. Salmen, U. Beisiegel, H. Weller, *Nano Lett.* **2009**, *9*, 4434.
[21] F. Hu, Q. Jia, Y. Li, M. Gao, *Nanotechnology* **2011**, *22*, 245604.
[22] B. H. Kim, N. Lee, H. Kim, K. An, Y. I. Park, Y. Choi, K. Shin, Y. Lee, S. G. Kwon, H. B. Na, J.-G. Park, T.-Y. Ahn, Y.-W. Kim, W. K. Moon, S. H. Choi, T. Hyeon, *J. Am. Chem. Soc.* **2011**, *133*, 12624.
[23] Z. Li, B. Tan, M. Allix, A. I. Cooper, M. J. Rosseinsky, *Small* **2008**, *4*, 231.
[24] M. Rohrer, H. Bauer, J. Mintorovitch, M. Requardt, H.-J. Weinmann, *Invest. Radiol.* **2005**, *40*, 715.
[25] M. P. Morales, S. Veintemillas-Verdaguer, M. I. Montero, C. J. Serna, *Chem. Mater.* **1999**, *11*, 3058.
[26] T. Çukur, M. Yamada, W. R. Overall, P. Yang, D. G. Nishimura, *Magn. Reson. Med.* **2010**, *63*, 427.
[27] F. Eibofner, G. n. Steidle, R. Kehlbach, R. d. Bantleon, F. Schick, *Magn. Reson. Med.* **2010**, *64*, 1027.
[28] A. Senpan, S. D. Caruthers, I. Rhee, N. A. Mauro, D. P. J. Pan, G. Hu, M. J. Scott, R. W. Fuhrhop, P. J. Gaffney, S. A. Wickline, G. M. Lanzat, *ACS Nano* **2009**, *3*, 3917.
[29] I. Hussain, S. Graham, Z. X. Wang, B. Tan, D. C. Sherrington, S. P. Rannard, A. I. Cooper, M. Brust, *J. Am. Chem. Soc.* **2005**, *127*, 16398.
[30] Z. X. Wang, B. E. Tan, I. Hussain, N. Schaeffer, M. F. Wyatt, M. Brust, A. I. Cooper, *Langmuir* **2007**, *23*, 885.
[31] X. Huang, Y. Luo, Z. Li, B. Li, H. Zhang, I. Majeed, P. Zou, B. Tan, *J. Phys. Chem. C* **2011**, *115*, 16753.